ORIGINAL PAPER

A polyethylene glycol (PEG) – polyethersulfone (PES)/multi-walled carbon nanotubes (MWCNTs) polymer blend mixed matrix membrane for CO_2/N_2 separation

Kar Kit Wong[1] · Zeinab Abbas Jawad[1,2] · Bridgid Lai Fui Chin[1]

Abstract

Recently, carbon capture utilizing membrane technology has received much attention to limit the adverse effect caused by rising carbon dioxide (CO_2) concentration in the atmosphere as they are less energy intensive and more environmentally friendly. Among the type of membranes, mixed matrix membranes (MMMs) has shown promising gas separation results. In this study, polymer blend MMMs were fabricated using polyethylene glycol (PEG), polyethersulfone (PES), multi-walled carbon nanotubes (MWCNTs) and solvent N,N-dimethylformamide (DMF) using wet phase-inversion technique. Results shown that functionalized MWCNTs (MWCNTs-F) were able to enhance gas separation performance of MMM. Furthermore, the effect of MWCNTs-F loading (0.005 wt% to 0.03 wt%) and polymer composition (PEG-PES weight ratio of 20:20, 30:10 and 32:8) were also studied. Results shown both parameters affect the gas separation performance of MMMs. The best performance in term of CO_2/Nitrogen (N_2) selectivity is found to be 1.235 ± 0.002 for MMM fabricated with 30 wt% PEG, 10 wt% PES and 0.02 wt% MWCNTs-F. In addition, MMM synthesized with PEG-PES weight ratio of 20:20 can withstand a pressure of 1.2 bar, indicating high mechanical strength. Hence, it is applicable in the post combustion carbon capture industry as typical flue gas has a pressure of 1.01 bar.

Keywords Polyethylene glycol (PEG) · Polyethersulfone (PES) · Functionalized carbon nanotubes (MWCNTs-f) · Mixed matrix membranes (MMMs) · Carbon capture

Nomenclature

ATR-FTIR	Attenuated total reflectance fourier transform infrared
CNTs	Carbon nanotubes
CO_2	Carbon dioxide
DMF	N,N-dimethylformamide
MMM	Mixed matrix membrane
MMMs	Mixed matrix membranes
MWCNTs	Multi-walled carbon nanotubes
MWCNTs-F	Functionalized multi-walled carbon nanotubes
N_2	Nitrogen
PEG	Polyethylene glycol
PES	Polyethersulfone
SEM	Scanning Electron Microscopy
TEM	Transmission Electron Microscopy
β-CD	Beta-cyclodextrin

✉ Zeinab Abbas Jawad
zeinab.aj@curtin.edu.my

[1] Department of Chemical Engineering, Faculty of Engineering and Science, Curtin University Malaysia, 250 CDT, 98009 Miri, Sarawak, Malaysia

[2] Department of Chemical Engineering, College of Engineering, Qatar University, Doha, Qatar

Introduction

Atmospheric carbon dioxide (CO_2) concentration has been on the rise since the industrial revolution. This has led to global warming [1]. Several techniques have been utilized to reduce the industrial CO_2 emission. Amine absorption as post combustion carbon capture method is a mature and well-commercialized technology but there are drawbacks as it is corrosive and energy intensive [2]. Hence, other techniques are studied for their potentiality in the industry as carbon capture [2].

One of these technologies is membrane gas separation which has been commercialized for selected gas separation processes such as acid gas removal and air separation since

the last two to three decades [3]. Nevertheless, there are challenges in developing an effective carbon capture membrane which are the inverse relationship between permeability and selectivity [3]. Recently, mixed matrix membranes (MMMs) has gained much attention as they incorporate the advantages from both organic and inorganic materials. However, MMMs faces challenges such as poor interaction between polymer phase and inorganic phase, interfacial defects and dispersion issues [4]. These causes the performance of MMMs in gas separation to decrease [4]. Therefore, it is necessary to investigate alternative polymer and filler pairs to improve CO_2/Nitrogen (N_2) separation of MMMs.

Polyethylene glycol (PEG) and polyethersulfone (PES) are frequently used in the gas separation industry to fabricate membranes [5]. PEG is known for its CO_2 affinity which attributes to high CO_2 permeability in PEG-based membrane [6]. However, high crystallinity of PEG affects the permeability as the crystalline phase hinders diffusion of molecule through the membrane [7]. On the other hand, PES is well-known for its chemical and mechanical stability and providing an additional binding mode for CO_2 molecules through the presence of ether unit in the polymer [8, 9].

Carbon nanotubes (CNTs) have attracted much attention and are widely studied in the field of chemistry, physics, and material science due to their unique mechanical, electrical, and thermal properties that offers a wide range of application [10, 11]. However, CNTs has difficulties in dispersing in organic solvent and form agglomerate clusters [12, 13]. Hence, many efforts have been taken to functionalize or modify CNTs to improve their dispersibility in organic solvent [12–14].

In another study, Ismail et al. (2011) incorporated multiwalled carbon nanotubes (MWCNTs) into PES membrane [15]. The effect of MWCNTs content in MMMs was investigated. They have found that MMM embedded with 0.5% MWCNTs has the highest CO_2/N_2 gas selectivity of 23.41. The gas selectivity reduced when MWCNTs loading was increased possibly due to formation of interfacial voids at higher loadings [15]. Furthermore, in a different study, Akbarian et al. (2018) have investigated the effect of polymer concentration on gas separation of blend membrane [5]. They have found that blend membrane with 30 wt% PEG 10,000 and 10 wt% PES has CO_2/N_2 selectivity enhanced 64% compared to pure PES membrane [5].

The main aim of this present work is to fabricate a high performance MMM from PEG 2000 and PES polymers with functionalized MWCNTs (MWCNTs-F) for CO_2/ N_2 separation. To date, polymer blend MMMs fabricated from PEG 2000 and PES polymers and MWCNTs for gas separation has not been studied. Additionally, no literature has reviewed the effect of different concentration of the polymers in PEG-PES-based MMMs. Both PEG and PES are common polymeric materials used in the membrane industries. PEG has

a strong affinity towards CO_2 molecules due to the presence of polar ether group in the molecule. Furthermore, PES is known for its thermal stability, chemical resistance, processability and gas separation properties. In addition, the presence of ether-oxygen unit in the molecule provides a binding mode for CO_2.

Experimental work

Materials

PES and PEG (PEG 2000) polymers was purchased from Sigma-Aldrich, Malaysia. MWCNTs (95% purity) with average inner and outer diameter of 8.85 nm and 26.62 nm, respectively were acquired from Shenzhen Nanotech Port Co. Ltd, China. Beta-cyclodextrin (β-CD), ethanol and solvent N,N-dimethylformamide (DMF), ACS reagent $\geq$ 99,7%, were purchased from Merck, Malaysia.

Functionalization of MWCNTs (MWCNTs-F)

Chen's soft cutting method was utilized to functionalize MWCNTs with the use of β-CD as the functionalizing agent [16]. MWCNTs were first dried overnight in a 120 °C oven to remove moisture [17]. 1 g of MWCNTs and 30 g of β-CD was grounded with an agate mortar and pestle for 10 min coupled with gradual addition of ethanol until a viscous greyish mixture was formed [16]. The mixture was then further grounded for another 2.5 h without addition of ethanol to obtain a homogeneous fine grey powder. The powder was then heated in an 80 °C oven for 24 h to obtain MWCNTs-F [17].

Preparation of membranes

Blend membrane of PEG-PES were prepared via wet-phase inversion method. PEG and PES were dissolved in DMF and continued stirred for 4 h at 750 rpm [5]. The casting solution was then sonicated using an ultrasonic degasser at room temperature for 10 min to removes gas bubbles [12]. A membrane film with 250 μm thickness is casted onto a glass plate using a membrane casting machine. The film was immediately immersed in distilled water at room temperature for 24 h to demix the casting solution and precipitate the membrane. The membrane was then dried in an oven for 24 h. The dried membrane was then stored in an airtight container until used.

To prepare PEG-PES/MWCNTs MMMs, a suspension of DMF and MWCNTs was prepared by sonication for 20 min and then stirred using a mechanical stirrer with a speed of 750 rpm for 4 h to distribute the MWCNTs evenly [12, 17]. PEG and PES was then added and continued stirred

Table 1 The composition of membranes

Membranes	Polymer (wt%)			Total Filler[a] (wt%)	MWCNTs-F (wt%)		Solvent (wt%)
	PEG	PES	Total		MWCNTs[b]	β-CD[c]	DMF
PEG-PES Blend	30	10	40	0.000	0.0000	0.0000	60.0000
MMM-0.005F	30	10	40	0.005	0.0020	0.0601	59.9379
MMM-0.01F	30	10	40	0.010	0.0040	0.1204	59.8756
MMM-0.02P	30	10	40	0.020	0.0080	0.0000	59.9920
MMM-0.02F	30	10	40	0.020	0.0080	0.2415	59.7505
MMM-0.03F	30	10	40	0.030	0.0121	0.3634	59.6245
MMM-PEG1	20	20	40	0.020	0.0080	0.2415	59.7505
MMM-PEG2	32	8	40	0.020	0.0080	0.2415	59.7505

[a] Total filler = amount of MWCNTs incorporated into polymer blend

[b] $MWCNTs = \dfrac{\left(\frac{TotalFiller}{100}\right)(TotalPolymer)}{\left[1 - \frac{TotalFiller}{100}(1+30)\right]}$

[c] β-CD = 30 × MWCNTs

for another 4 h at 750 rpm. The casting and drying steps were performed as described previously. The composition of MMMs synthesized for this study were summarized in Table 1.

Single gas permeation test

Single permeation tests using pure N_2 and CO_2 at room temperature were carried out on the experimental setup illustrated schematically in Fig. 1 [17]. Each of the gas was supplied by a compressed gas cylinder in which the flowrate was controlled at 100 mL/min by a mass flow controller (Aalborg AFC26, USA). The feed flowrate was displayed and controlled by connecting the mass flow controller to a two-channel digital set point/readout unit (Aalborg 0 – 200 mL, USA). The feed gas pressure was varied between 0.25 – 3 bars for the testing. Pure N_2 was first used to purge the system for 15 min to ensure no contaminants. The prepared membrane sample was then cut into round disc shape with an effective area of 7.07 cm^2 and placed in the membrane permeation cell which was locked tightly before connecting it back to the experimental rig.
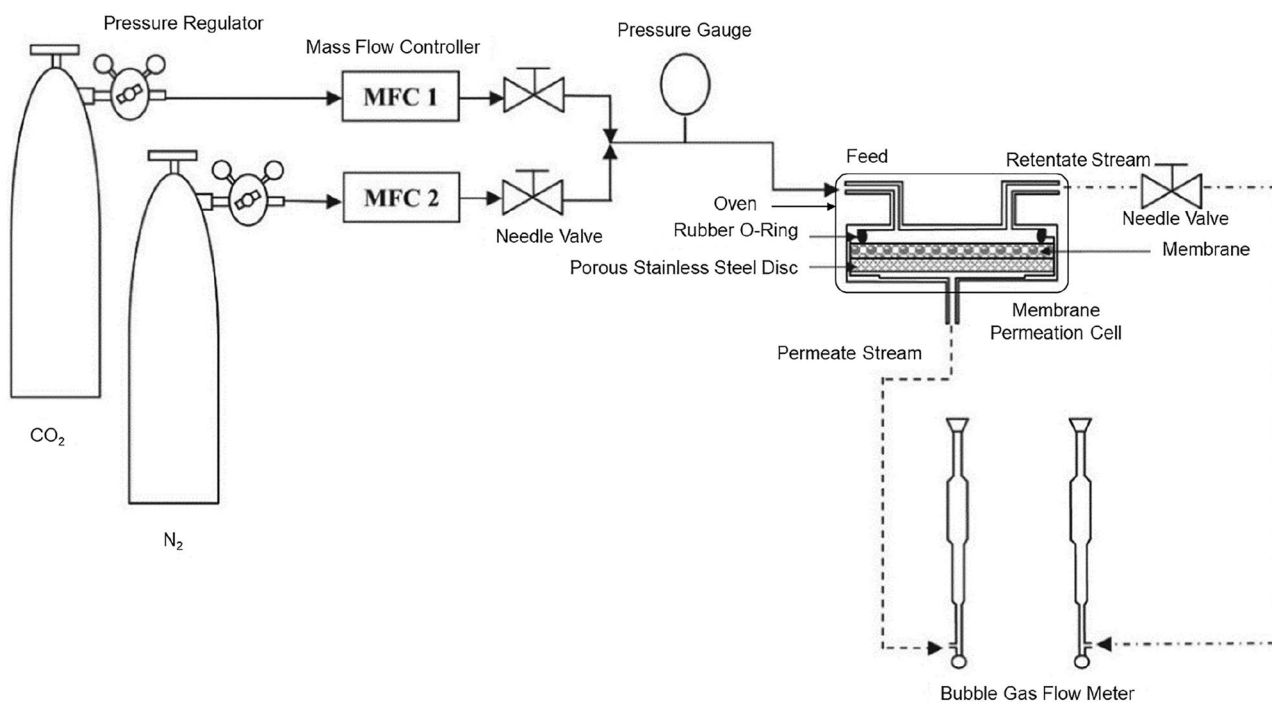
Fig. 1 Schematic Diagram of Experimental Rig Setup [17]

A gas leak detection test was performed on the testing rig to ensure no feed gas escape from the connecting pipes of the rig before the permeation test was carried out. The bubble gas flow meter was used to obtain the gas permeance volume displacement while a stopwatch was used to measure the displacement time.

The permeance of the membrane (P/l) expressed in GPU can be calculated using Eq. 1 below [17].

$$\frac{P}{l} = \frac{Q}{A\Delta p} \tag{1}$$

where,

l is the membrane thickness (cm)

Q is the measured volumetric flowrate (cm^3/s)

A is the effective membrane area (cm^2)

Δp is the pressure difference across the membrane (cmHg)

Meanwhile, the selectivity of the membrane for CO_2 over N_2 can be calculated using the ideal separation factor in Eq. 2 below [17].

$$\alpha_{CO_2/N_2} = \frac{P_{CO_2}}{P_{N_2}} = \frac{(P/l)_{CO_2}}{(P/l)_{N_2}} \tag{2}$$

where,

P_{CO2} is the permeability of CO_2 gasses through the membrane

P_{N2} is the permeability of N_2 gasses through the membrane

Characterization of MMMs

Transmission electron microscopy (TEM)

The morphology of MWCNTs and MWCNTs-F were characterized using TEM (Philips CM12) equipped with DOCU version 3.2 image analysis systems.

Scanning electron microscopy (SEM)

The morphology and cross-sectional structure of the PEG-PES/MWCNTs MMMs synthesized were characterized using a SEM (Hitachi TM3000, Tokyo, Japan). All the membranes sample were frozen overnight in a cryogenic freezer at -80 °C. The membrane samples were then fractured. To avoid samples having charges that causes contrasting images, the cracked membranes were coated with platinum sputtering before being observed with the SEM. At least 5 samples were characterized in order to check its reproducibility.

Attenuated total reflectance fourier transform infrared spectroscopy (ATR-FTIR)

The presence of functional groups in the fabricated PEG-PES/MWCNTs MMMs were characterized using Thermo Scientific Fourier Transform Infrared Spectrometer (Nicolet IS10, USA) with wavelength of 400 to 4000 cm^{-1}. Data was obtained with 32 scans of 4 cm^{-1} resolution for each spectrum using a diamond crystal. The background information of the room condition was first obtained and repeated three times before collecting data for each sample.

Results and discussion

Development of MWCNTs-F

Pristine MWCNTs and MWCNTs-F were observed using TEM as shown in Fig. 2. Pristine MWCNTs has an average inner and outer diameter of 8.85 nm and 26.62 nm were observed to be agglomerated in Fig. 2a. Furthermore, surface defects and impurities (black dots) were present on the outer surface and inside of the carbon nanotubes. Besides the defective structure, the pristine MWCNTs were found to be close ended, which impacts the gas separation property of MWCNTs [12, 18].

After functionalization with β-CD, the MWCNTs-F are less agglomerated and shorter (Fig. 2b) compared to pristine MWCNTs (Fig. 2a). This is due to the repelling effect among MWCNTs-F which is caused by hydrogen bonding and Wan der Waal interactions between adjacent β-CD that are coated on the outer walls of the MWCNTs [12]. The outer diameter of MWCNTs has also been increased to 39.17 ± 0.18 nm (Fig. 2c). This increase in the diameter of CNTs is due to the uniform coating of β-CD. Furthermore, an open-ended structure can be observed in Fig. 2c due to the soft-cutting method procedure that leaves MWCNTs open-ended when they are cut [12, 19].

Effect of integration of MWCNTs within PEG-PES blend membrane

Attenuated total reflectance fourier transform infrared (ATR-FTIR) spectroscopy analysis

Functional groups presence in the PEG-PES blend membrane and MMMs incorporated with MWCNTs and MWCNTs-F were analysed using ATR-FTIR. Figure 3 depicts organic functional groups in the blend membrane and MMMs. Presence of PES in the MMMs was verified through the presence of benzene ring, ether (C-O) and sulfone (S=O) functional group shown in Fig. 3. Three peaks ranging from 1600 cm^{-1} to 1400 cm^{-1} (1577 cm^{-1},
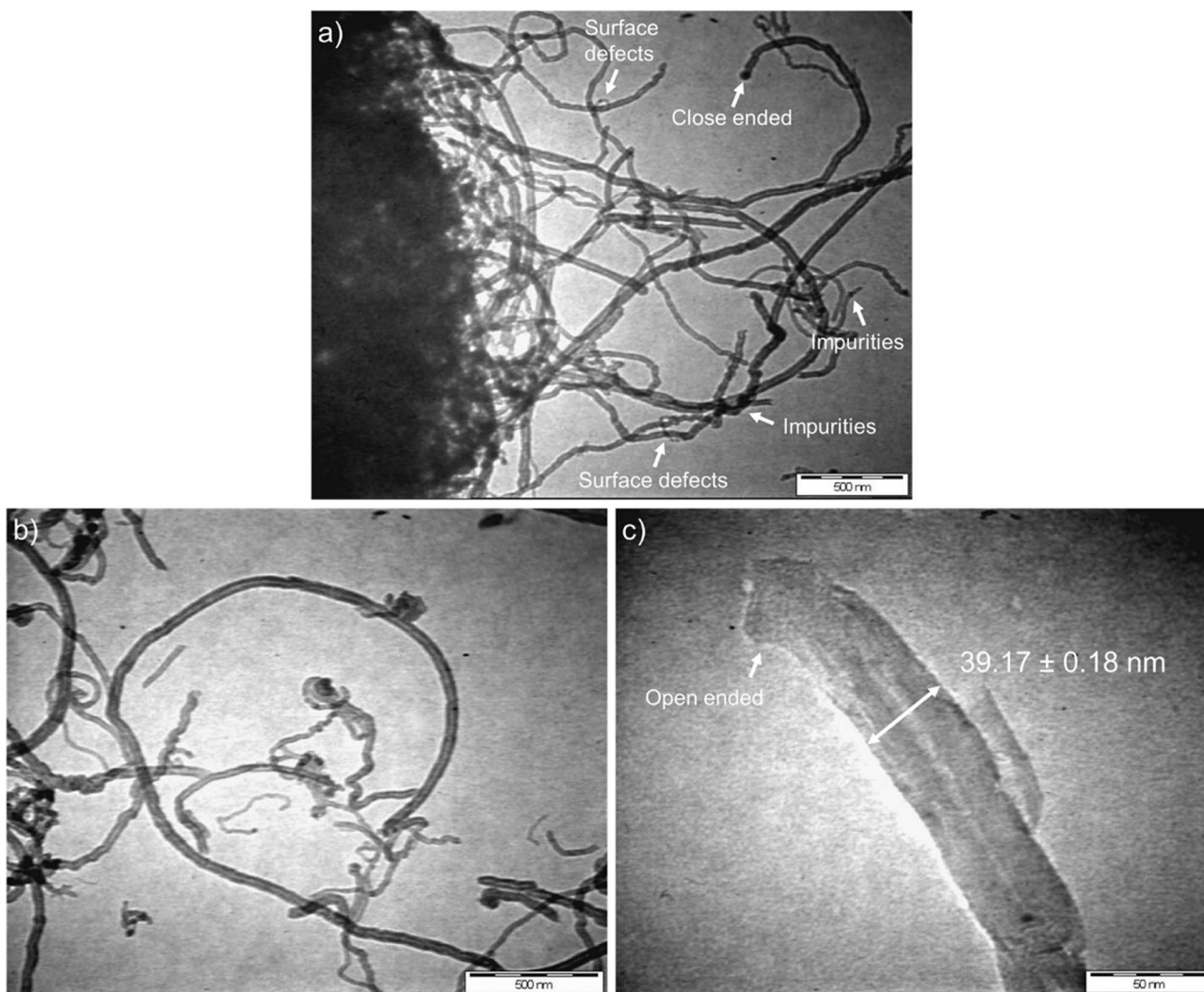
Fig. 2 TEM images of (**a**) Pristine MWCNTs and (**b-c**) MWCNTs-F

1485 cm^{-1} and 1406 cm^{-1}) and $=$ C–H vibration indicated at 3068 cm^{-1} confirm the presence of benzene ring [5, 20]. In addition, stretching peaks at 1322 cm^{-1}, 1298 cm^{-1}, and 1238 cm^{-1} corresponds to C–O group while stretching peaks at 1149 cm^{-1} and 1104 cm^{-1} have proven the presence of S $=$ O group. Furthermore, hydroxyl (–OH) and alkanes (–CH$_2$) groups presence in PEG polymer can be seen through the peak at 3542 cm^{-1} and 2871 cm^{-1}, respectively [5, 21]. Furthermore, presence of C–O–C group in the blend membrane and MMMs contributed to the stretching peak at 1011 cm^{-1} [22]. The heightened intensity of both C–C and O–H stretching peaks for MMM-0.02F compared to PEG-PES blend membrane and MMM-0.02P is due to the -OH group presence in β-CD used as functionalization agent for MWCNTs and the presence of benzene ring in MWCNTs-F [17, 23].

Scanning electron microscopy (SEM)

Figure 4 presents the surface and cross-section morphologies of PEG-PES blend membrane and MMMs integrated with MWCNTs and MWCNTs-F. Figure 4b, d and f show the asymmetric structure of a dense top layer followed by propagation of finger-like structure and sponge-like structures near the bottom can be observed across all the membranes. The formation of finger-like structures is a result of instantaneous demixing causing precipitation of polymer and rapid formation of solid film [24]. Sponge-like structure can be observed between the finger-like macrovoids and towards the bottom of the membranes are attributed to the precipitated nuclei formed by impeded nonsolvent influx [25, 26]. Compared to PEG-PES blend membrane (Fig. 4b), MMM incorporated with MWCNTs has defective
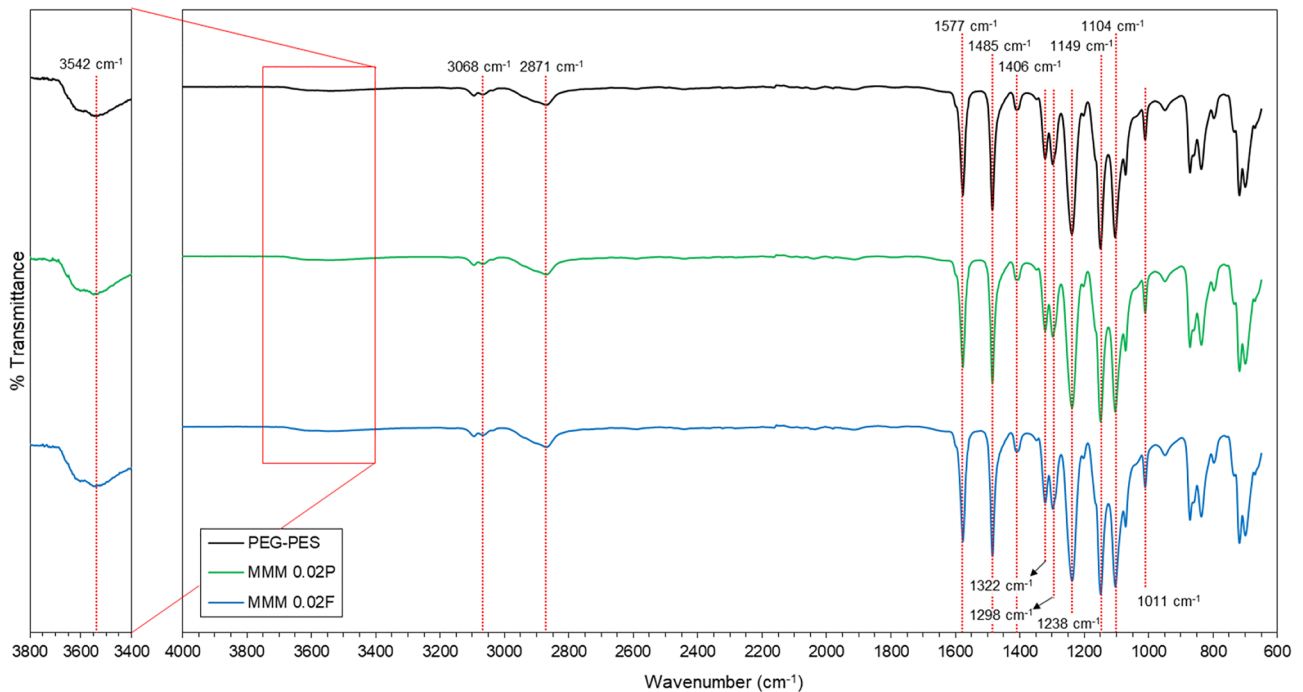
Fig. 3 ATR-FTIR of PEG-PES blend membrane and MMMs incorporated with pristine and functionalized MWCNTs at casting thickness of 250 μm
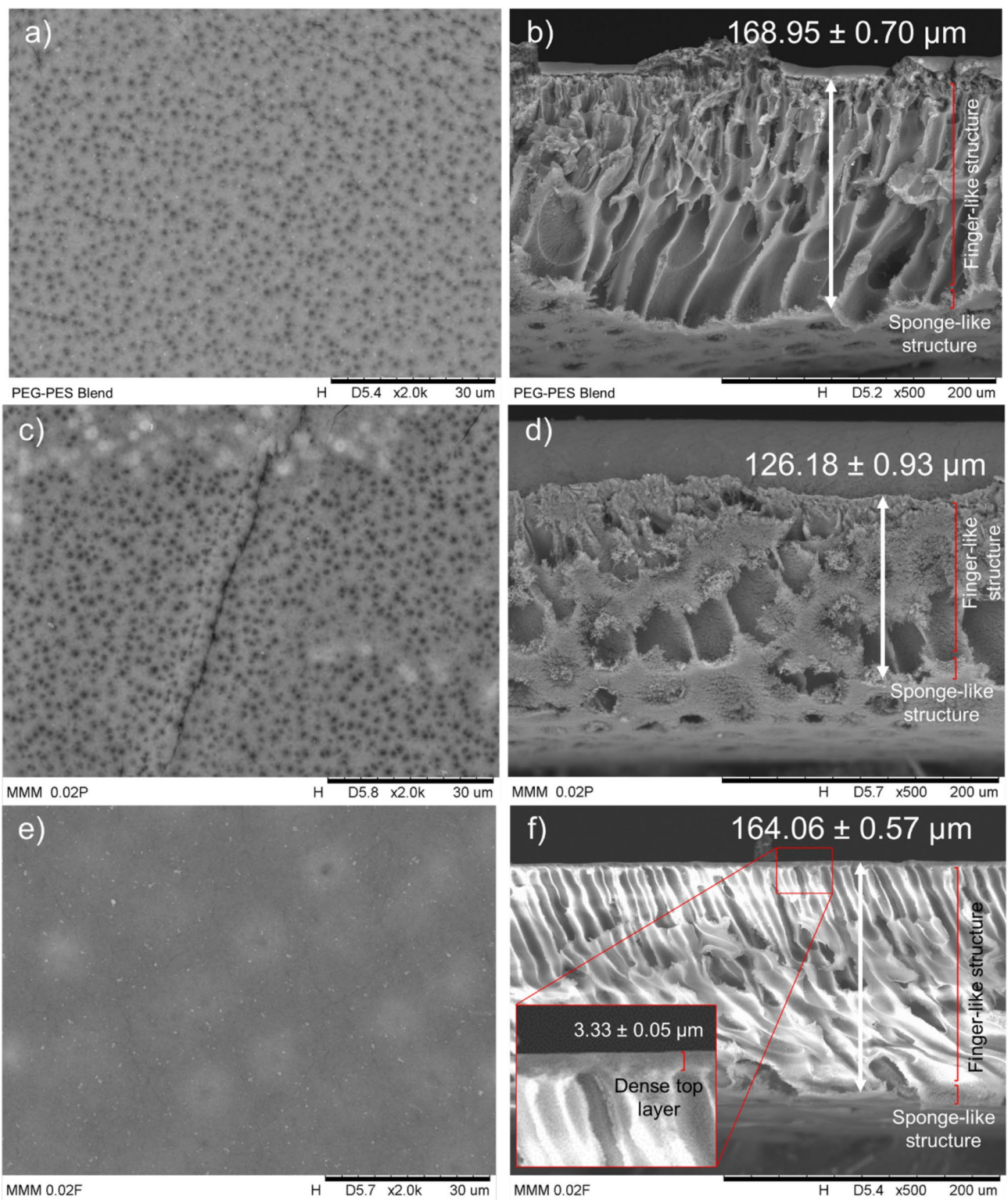
agglomerated cross-sectional morphology as seen in Fig. 4d. MWCNTs agglomerate because of the poor interaction with polymer matrix and having stronger π–π interaction with each other [27]. Besides, the high ratio of length to diameter of MWCNTs contributes to agglomeration as they are susceptible to entanglement [28]. Contrary, Fig. 4f shows no sign of agglomeration when MMM was incorporated with MWCNTs-F. According to Ahmad et al. (2014), the dispersibility of MWCNTs is enhanced through the repelling behaviour of MWCNTs-F caused by hydrogen bonding and Van der Waals interactions between adjacent coating of β-CD on MWCNTs-F [12]. Furthermore, a 3.33 ± 0.05 μm dense top layer can be seen in Fig. 4f. The formation of dense top layer is due to β-CD presence in MWCNTs-F coalescing polymer chain [19].

CO$_2$ and N$_2$ separation performance

The effect of integrating MWCNTs within PEG-PES blend membranes were studied by performing single permeation test of CO$_2$ and N$_2$. Figure 5 presents the CO$_2$ permeance of the synthesized membranes. Incorporation of 0.02 wt% of MWCNTs in MMMs had decreased the CO$_2$ permeance from $12,469.71 \pm 11.22$ GPU of PEG-PES blend membrane to 9333.40 ± 3.62 GPU. This may due to the agglomeration of MWCNTs [29]. Agglomerated MWCNTs seen in Fig. 4d have reduced pore accessibility for CO$_2$ that allow rapid gas transport [28]. Compared

to PEG-PES blend membrane and MMM-0.02P, MMM incorporated with 0.02 wt% MWCNTs-F has higher CO$_2$ permeance of $12,594.28 \pm 22.77$ GPU. This shows that MWCNTs-F are better at enhancing gas separation than MWCNTs as MWCNTs functionalized through Chen's soft cutting method using β-CD shortened the MWCNTs and improved dispersibility of MWCNTs in the polymer matrix [12]. With MWCNTs-F dispersed without agglomerating in the polymer phase, as confirmed in Fig. 4f, CO$_2$ molecules were able to access to the nanochannels of CNTs for rapid gas transport, improving CO$_2$ permeance [28]. Furthermore, Ge et al. (2011) suggested that interaction between polymer-chain segment and carbon nanotubes (CNTs) plays a major role in enhancing gas permeation by disrupting polymer-chain packing that increases total free volume [30].
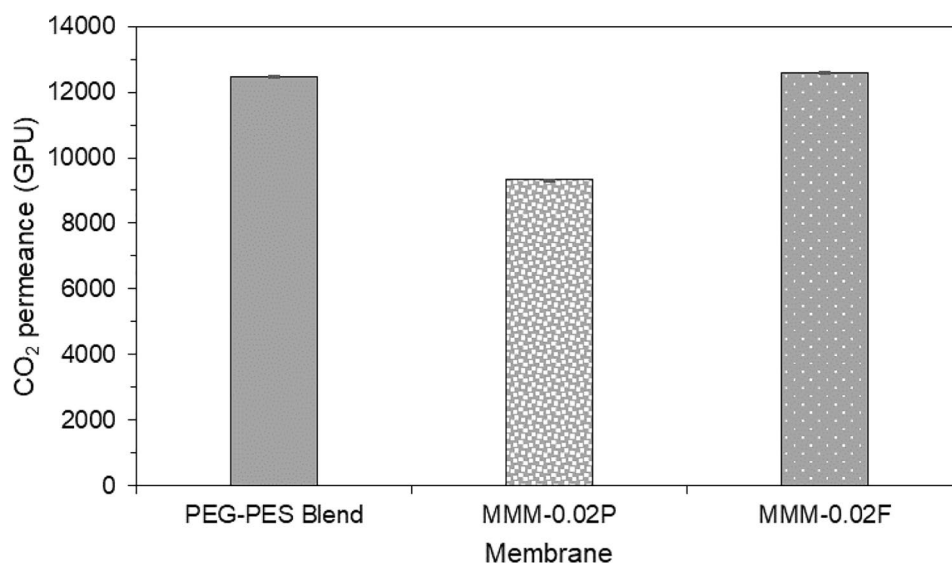
The N$_2$ permeance for the synthesized membranes are illustrated in Fig. 6. According to Fig. 6, both MMM-0.02P and MMM-0.02F have a lower N$_2$ permeance of 9839.64 ± 10.49 GPU and $10,197.53 \pm 22.77$ GPU compared to PEG-PES blend membrane ($12,469.71 \pm 11.22$ GPU), respectively. Lowered N$_2$ permeance for MMM-0.02P can be explained by the rough aggregated structure of agglomerated MWCNTs that increases resistance to gas permeation, reducing N$_2$ permeance [28]. Meanwhile, for MMM-0.02F, the reduced N$_2$ permeance is mainly due MWCNTs-F that favour N$_2$ gas molecules less [17]. This is due to MWCNTs functionalized through Chen's soft cutting method have

Fig. 4 SEM surface and cross-sectional morphologies of (**a-b**) PEG-PES blend membrane and MMMs incorporated with (**c-d**) pristine and (**e–f**) functionalized MWCNTs, respectively at casting thickness of 250 μm

decreased the surface area and cumulative volume of pores of MWCNTs that contributes to N_2 adsorption [12].

Figure 7 illustrates the CO_2/N_2 selectivity for PEG-PES blend membrane, MMM-0.02P and MMM-0.02F. Incorporation of MWCNTs in PEG-PES blend membrane has reduced the CO_2/N_2 selectivity from 1.050 ± 0.001 to 0.949 ± 0.001. This may due to the aggregated pores of MWCNTs has high adsorption capacity of N_2 molecules [27]. Meanwhile, for MMM incorporated with 0.02 wt% MWCNTs-F, the CO_2/N_2 selectivity was higher at 1.235 ± 0.002. This increase in selectivity is associated with good compatibility between MWCNTs, β-CD and polymer matrix [17]. This contribute to the well dispersed MWCNTs-F, where smooth-walled MWCNTs provide rapid gas transport while β-CD

selectively encapsulate CO_2 molecules increasing CO_2/N_2 selectivity [12, 31].

Effect of different loading of MWCNTs-F in MMM

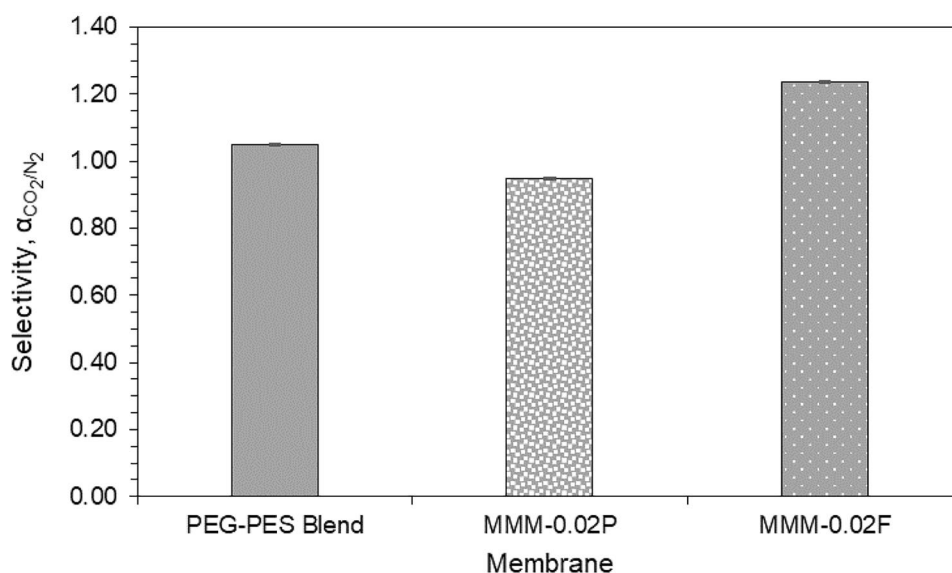### Attenuated total reflectance fourier transform infrared (ATR-FTIR) spectroscopy analysis

ATR-FTIR Spectroscopy was used to analyse the functional groups presence in the PEG-PES blend membrane and MMMs fabricated with 0.005 wt%, 0.01 wt%, 0.02 wt% and 0.03 wt% MWCNTs-F loading. The analysed organic functional groups in the blend membrane and MMMs are shown in Fig. 8.

Scanning electron microscopy (SEM)

Apart from the ATR-FTIR analysis, the surface and cross-sectional morphologies of the PEG-PES blend membrane, MMM 0.005F, MMM 0.01F, MMM-0.02F and MMM 0.03F were examined using SEM analysis, as illustrated in Fig. 9 to have a better understanding on the gas transport behaviour of the membranes. Figure 9b, d, f, h and j show the cross-sectional asymmetric structure of the membranes. The thickness of the dense top layer of the membrane increased from 2.89 ± 0.06 μm to 3.33 ± 0.05 μm when the filler loading increased from 0.01 wt% to 0.02 wt%. This is due to the presence of β-CD that coalesce the polymer chains in the skin layer, forming a thicker and denser skin layer [19]. The coalescing effect of β-CD attribute to its hydrophobic hollow cavity allowing polymer chains to be threaded into
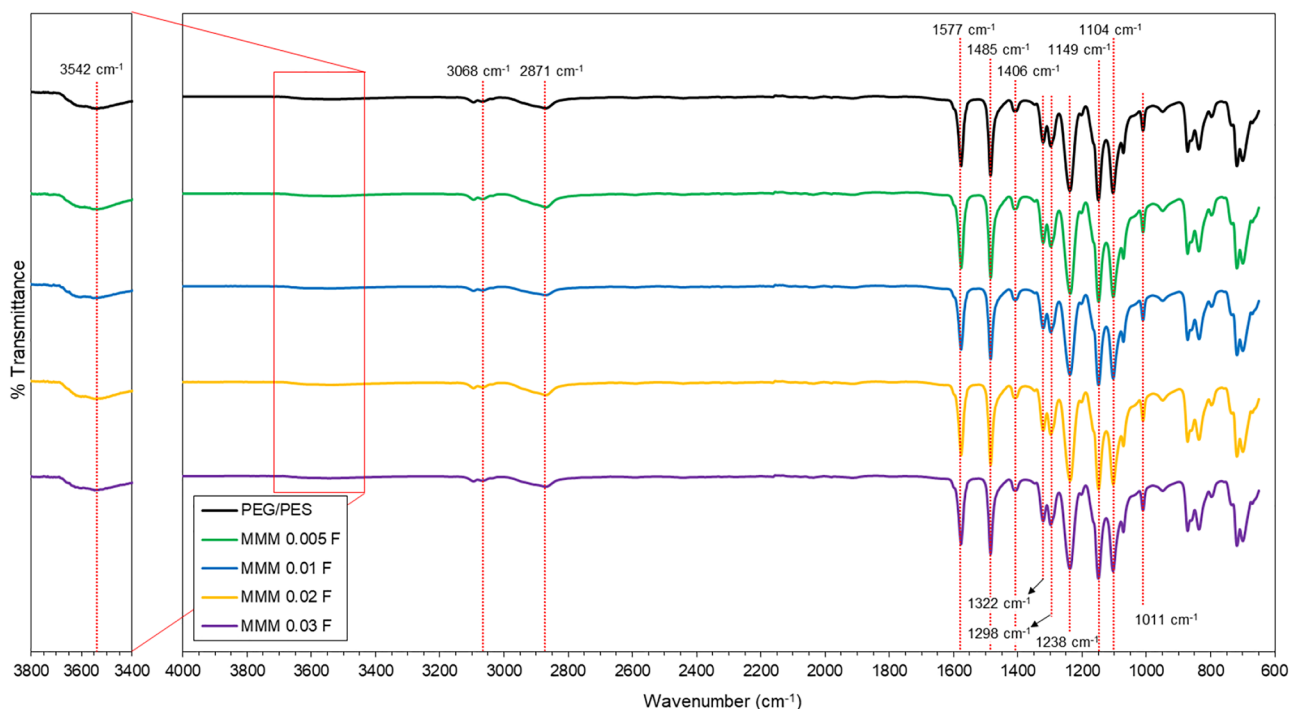
Fig. 8 ATR-FTIR of PEG-PES blend membrane and MMMs prepared with different filler loading of 0.005 wt%, 0.010 wt%, 0.020 wt% and 0.030 wt% at casting thickness of 250 μm
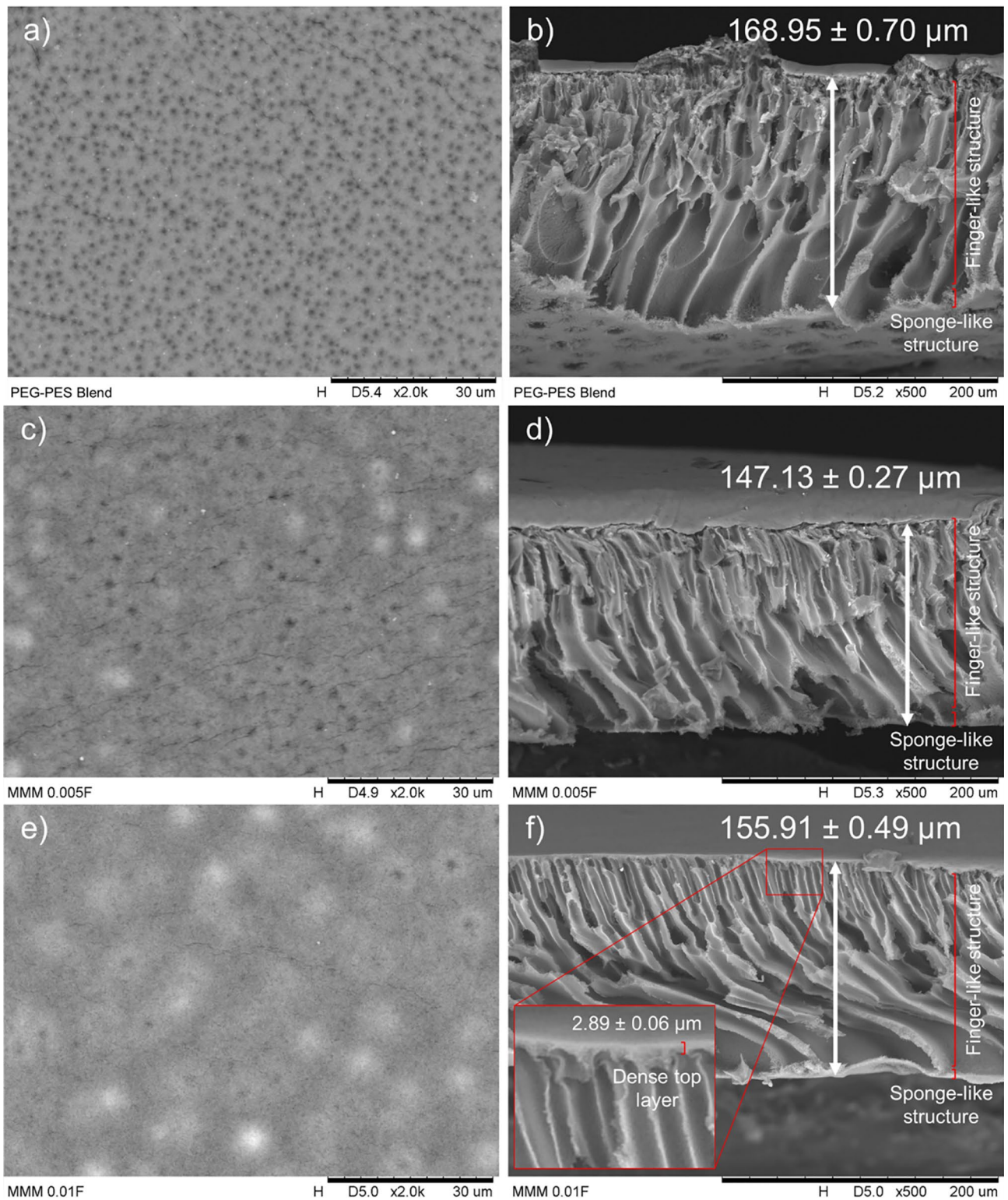
Fig. 9 SEM surface and cross-sectional morphologies of (**a-b**) PEG-PES blend membrane and MMMs prepared with different filler loading of (**c-d**) 0.005 wt%, (e–f) 0.010 wt%, (g-h) 0.020 wt% and (**i-j**) 0.030 wt% at casting thickness of 250 μm
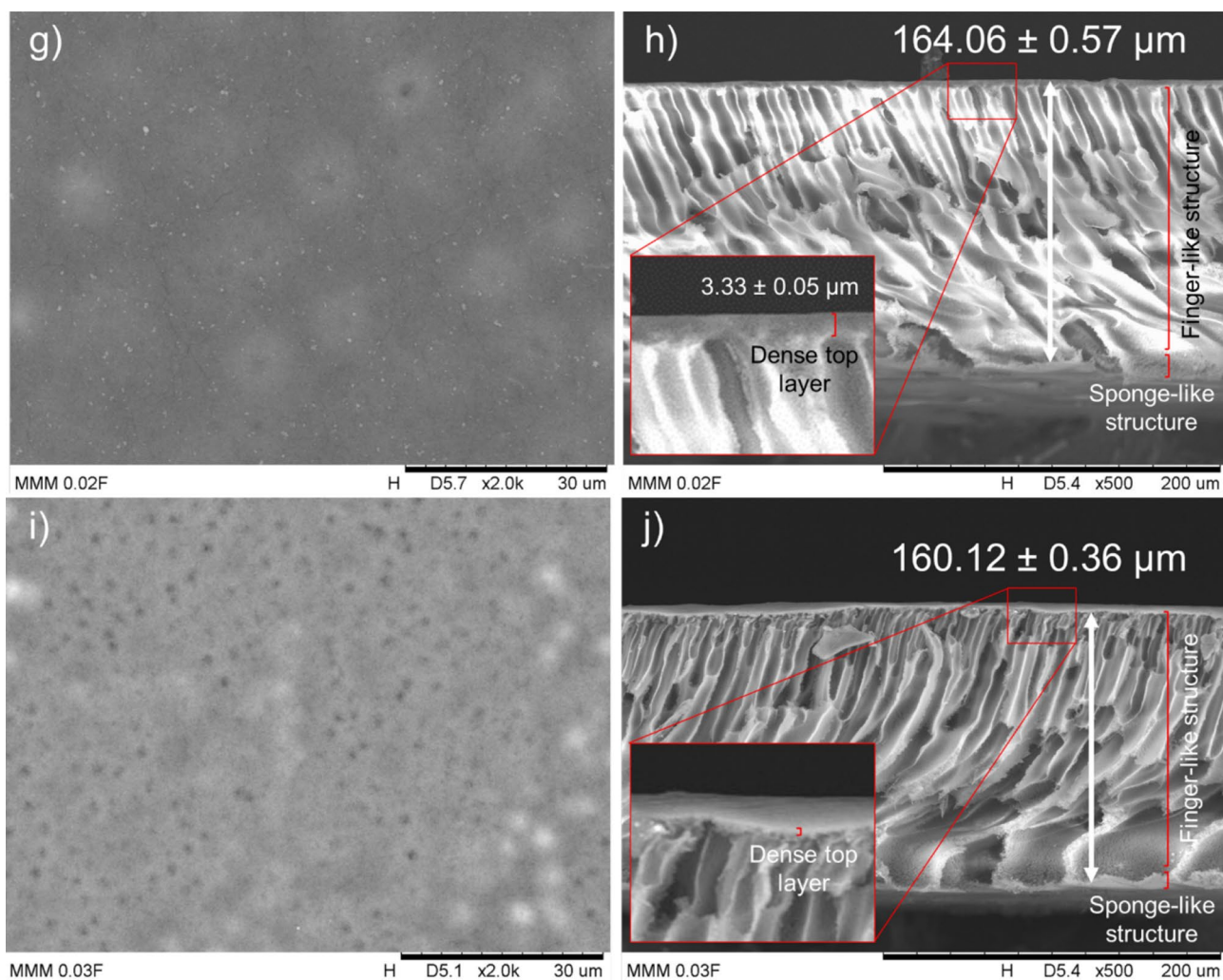
Fig. 9 (continued)

the cavity, resulting in a more intimate blend of polymers [32]. Interestingly, further addition of MWCNTs-F at 0.03 wt% has caused the thickness of dense top layer to reduce significantly, as seen in Fig. 9j. This may be explained by the uncontrolled loading of MWCNTs-F that causes agglomeration, reducing the available filler surface area to bond with the polymer chains [12]. Hence, the decreased bonding of β-CD with polymer chains may have reduced the coalescence effect of β-CD on polymer chain that aid formation of thicker skin layer.

CO_2 and N_2 separation performance

The effect of MWCNTs-F loading on the gas separation performance of membrane was studied by carrying out single permeation test of CO_2 and N_2. Figure 10 shows the effect of different MWCNTs-F loading on CO_2 permeance. Based on Fig. 10, the CO_2 permeance decreased

from $12{,}469.71 \pm 11.22$ GPU to $10{,}941.08 \pm 4.31$ GPU and 9142.94 ± 20.86 GPU when the filler loading is increased to 0.005 wt% and 0.010 wt%, respectively. This reduction in gas permeance can be explained by the presence of polymer chain rigidification [15]. Polymer chain rigidification is caused by the polymer-filler interaction, where mobility of the polymer chain segment is limited due to the adsorption of the polymer chain onto filler surface [15]. At 0.010 wt% filler loading, the CO_2 permeance was about 27% lower than the base polymer (0 wt% loading), which is in line with the reduction of 25%—33% permeance reported by other researchers when polymer rigidification occur [33]. However, further increase in filler loading shows a general increase in gas permeance up to $12{,}594.28 \pm 22.77$ GPU and $12{,}318.81 \pm 10.91$ GPU for 0.020 wt% and 0.030 wt%, respectively. The increase in CO_2 permeance is caused by the positive effect of MWCNTs-F on gas permeation outweighing the effect of rigidified polymers chain when MWCNTs-F

Fig. 10 CO_2 permeance of PEG-PES blend membrane and MMMs prepared with different filler loading of 0.005 wt%, 0.010 wt%, 0.020 wt% and 0.030 wt% at casting thickness of 250 μm at operating pressure of 0.25 bar
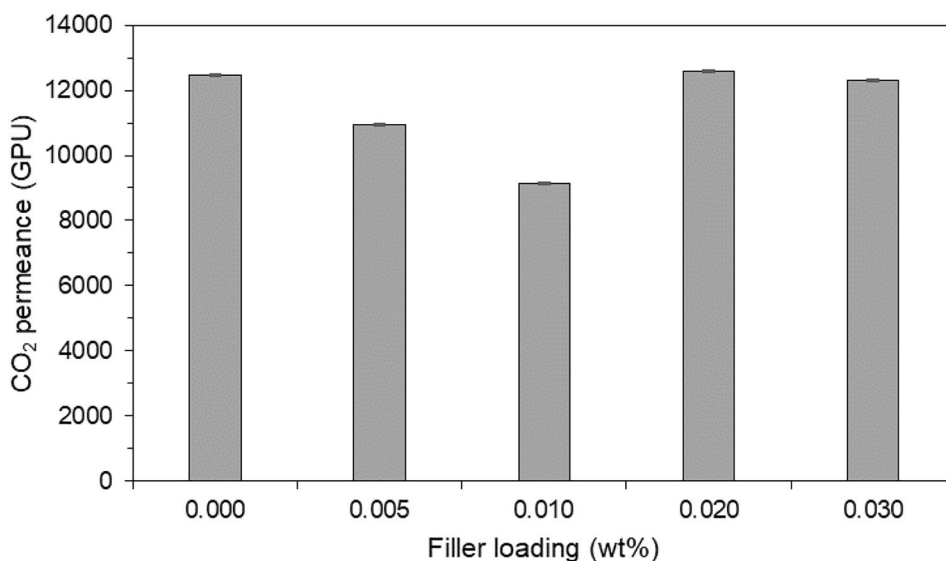
loading is high [15]. Compared to PEG-PES blend membrane, MMM-0.02F has higher CO_2 permeance attributes to the well incorporation of smooth surfaced MWCNTs-F in the MMM that act as nanochannels for rapid gas transport [12, 17].

The effect of different filler loading incorporated in MMMs on N_2 permeance are illustrated in Fig. 11. According to Fig. 11, the N_2 permeance decreased from $11,877.42 \pm 5.08$ GPU to 9924.07 ± 10.67 GPU and 7584.10 ± 14.36 GPU, when filler loading are increased to 0.005 wt% and 0.010 wt%, respectively. This is due to the limited chain mobility of rigidified polymer that reduces diffusivity of gas molecules [15]. However, at 0.010 wt% filler loading, the reduction of permeance compared to the base polymer (0.000 wt% filler loading) was 36%, higher than the

expected 25%—33% caused by polymer rigidification [33]. This may due to additional N_2 permeance limiting effect of non-covalent functionalized MWCNTs that selectively adsorb less N_2 molecules [17]. However, at 0.020 wt% and 0.030 wt% filler loading, the N_2 permeance is increased to $10,197.53 \pm 14.36$ GPU and $10,779.62 \pm 4.19$ GPU, respectively. This can be caused by the rapid gas transport effect of additional MWCNTs-F offsets the effect of lowered N_2 permeance caused by reduced polymer chain mobility [12, 15].

The effect of different MWCNT-Fs loading on CO_2/N_2 selectivity was observed in Fig. 12. The incorporation of MWCNTs-F into PEG-PES blend membrane has increased the CO_2/N_2 selectivity from 1.050 ± 0.001 to 1.102 ± 0.001, 1.206 ± 0.003 and 1.235 ± 0.002 at 0.005 wt%, 0.010 wt% and 0.020 wt%, respectively. The

Fig. 11 N_2 permeance of PEG-PES blend membrane and MMMs prepared with different filler loading of 0.005 wt%, 0.010 wt%, 0.020 wt% and 0.030 wt% at casting thickness of 250 μm at operating pressure of 0.25 bar
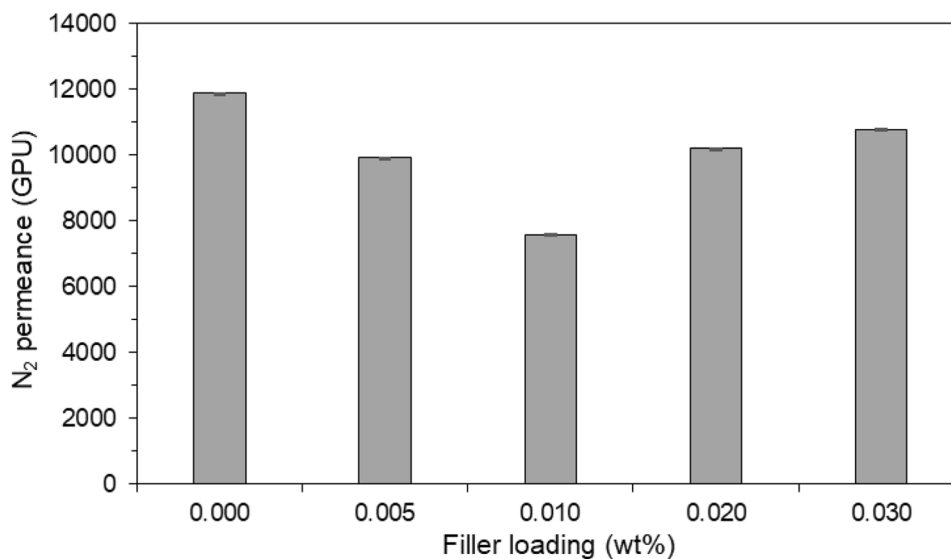
Fig. 12 CO_2/N_2 selectivity of PEG-PES blend membrane and MMMs prepared with different filler loading of 0.005 wt%, 0.010 wt%, 0.020 wt% and 0.030 wt% at casting thickness of 250 μm at operating pressure of 0.25 bar
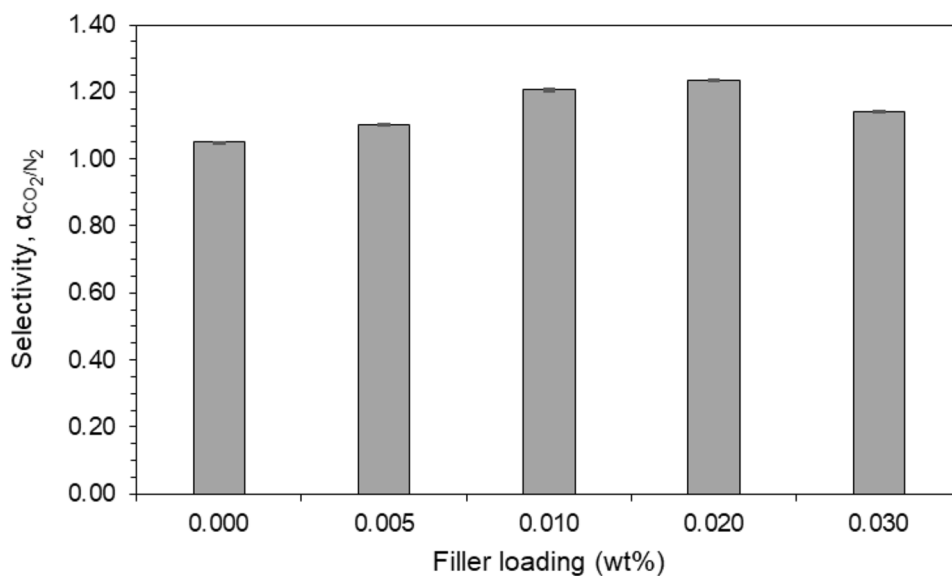

increase in CO_2/N_2 selectivity from 0.000 wt% to 0.020 wt% filler loading attribute to the increase in the thickness of the selective dense top layer, as confirmed in Fig. 9b, d, f and h. Furthermore, the increase in MWCNTs-F loading provided higher number of smooth nano-channel for gas transportation, while β-CD used to functionalize MWCNTs selectively encapsulate CO_2 molecules and reduce the solubility of N_2 molecules, increasing CO_2/N_2 selectivity [12, 31]. Meanwhile, when filler loading is increased to 0.030 wt%, the CO_2/N_2 selectivity is
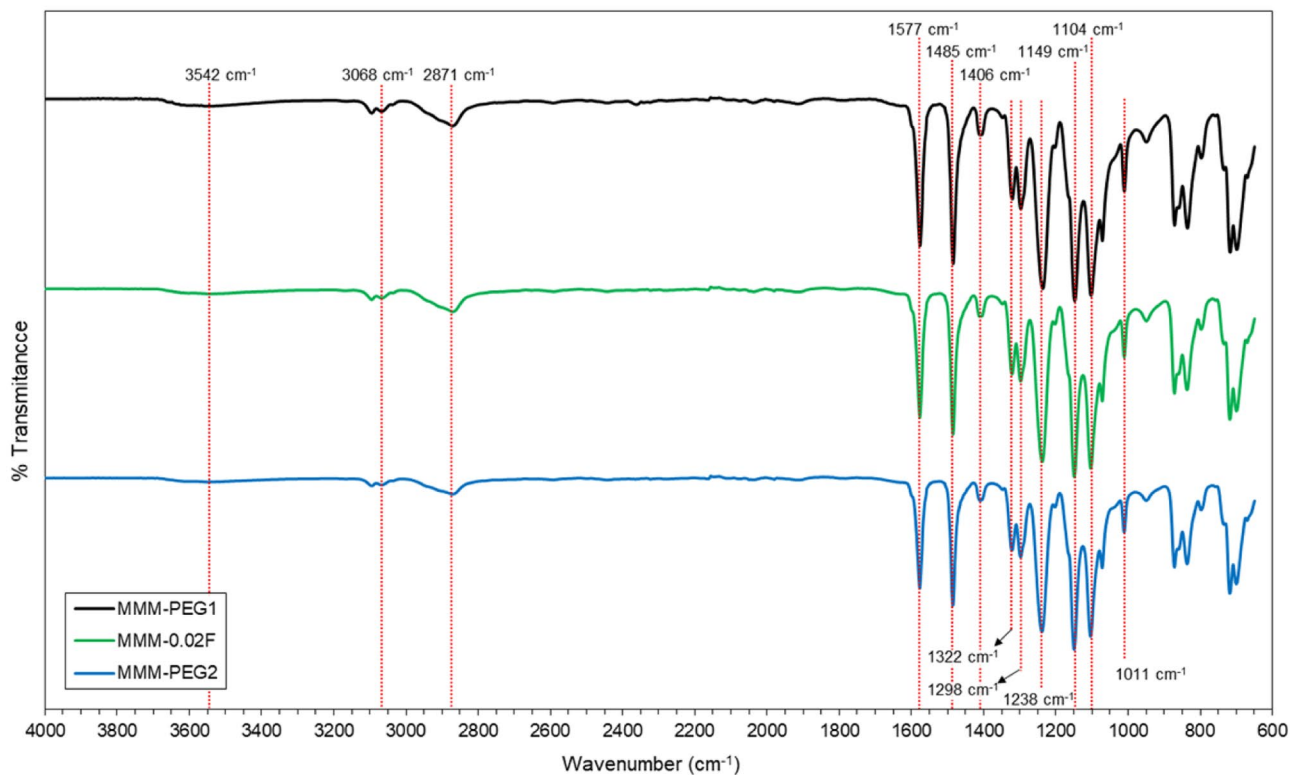
Fig. 13 ATR-FTIR of MMM-PEG1, MMM-0.02F and MMM-PEG2 prepared with PEG:PES weight ratio of 20:20, 30:10 and 32:8, respectively at casting thickness of 250 μm

decreased to 1.142 ± 0.001 due to the reduction in thickness of the dense top layer, as seen in Fig. 9j. Hence, the optimum filler loading found in this study is 0.020 wt% with selectivity of 1.235 ± 0.002.

Effect of polymer composition

### Attenuated total reflectance fourier transform infrared (ATR-FTIR) spectroscopy analysis

ATR-FTIR spectroscopy was used to analyze the organic functional group presence in MMM-PEG1, MMM-0.02F and MMM-PEG2 fabricated with PEG-PES weight ratio of 20:20, 30,10 and 32,8, respectively. Figure 13 presents the result of the analysis. The intensity of

C–C (1577 cm^{-1}, 1485 cm^{-1} and 1406 cm^{-1}) and S = O (1149 cm^{-1} and 1104 cm^{-1}) stretching peaks reduced from MMM-PEG1 to MMM-0.02F and MMM-PEG2. This is due to the lowered weight ratio of PES in the MMMs from 20 wt% to 10 wt% and 8 wt%, decreasing the presence of aromatic benzene ring and sulfone functional group of PES in the MMMs.

Scanning electron microscopy (SEM)

Figure 14 illustrates the surface and cross-section morphologies of MMM-PEG1, MMM-0.02F and MMM-PEG2 examined using SEM analysis. The cross-section morphologies of the asymmetric membranes are illustrated in Fig. 14b, d and f. The thickness of dense top layer decreased from 5.71 ± 0.10 μm to 3.33 ± 0.05 μm when PES is decreased

Fig. 14 SEM surface and cross-sectional morphologies of (**a-b**) MMM-PEG1, (**c-d**) MMM-0.02F and (**e-f**) MMM-PEG2 prepared with PEG:PES weight ratio of 20:20, 30:10 and 32:8, respectively at casting thickness of 250 μm
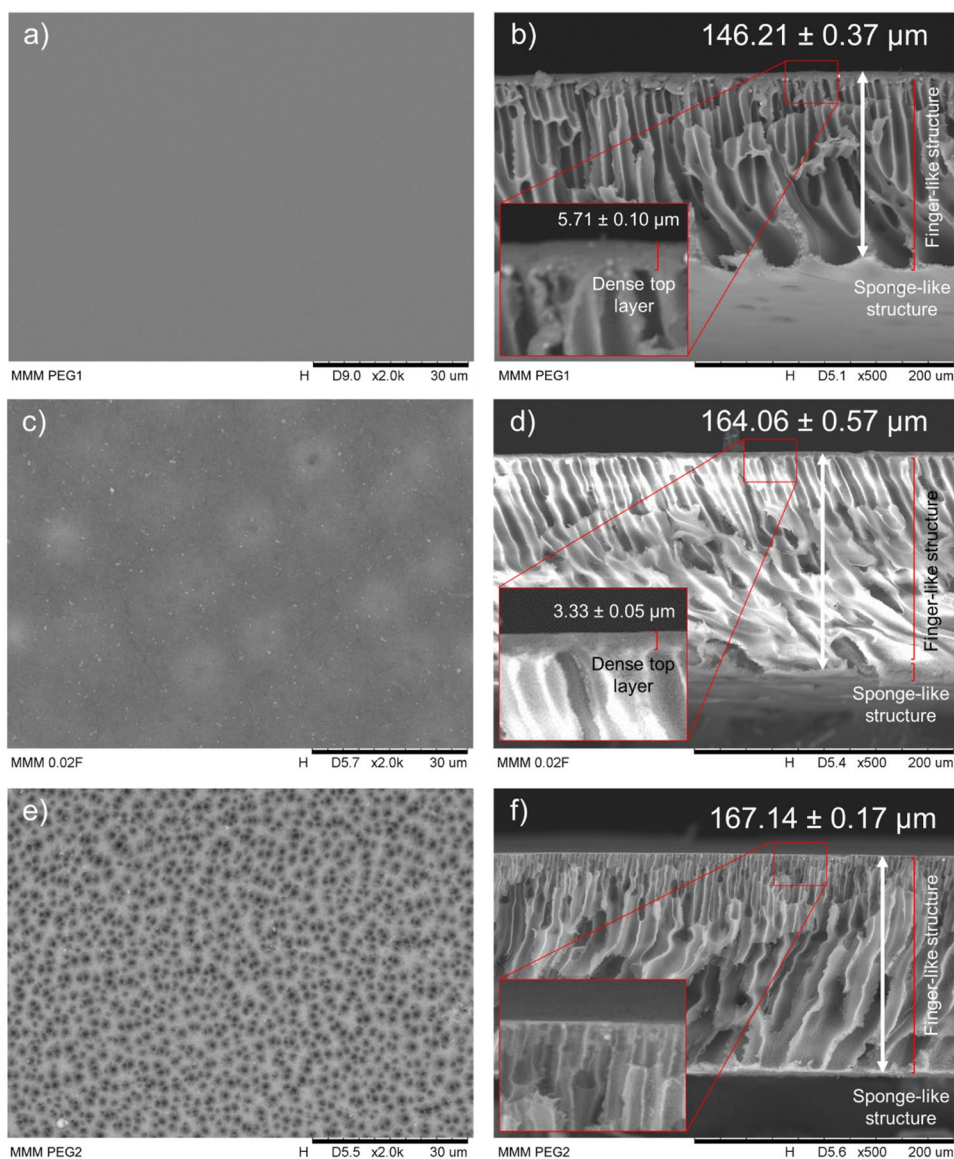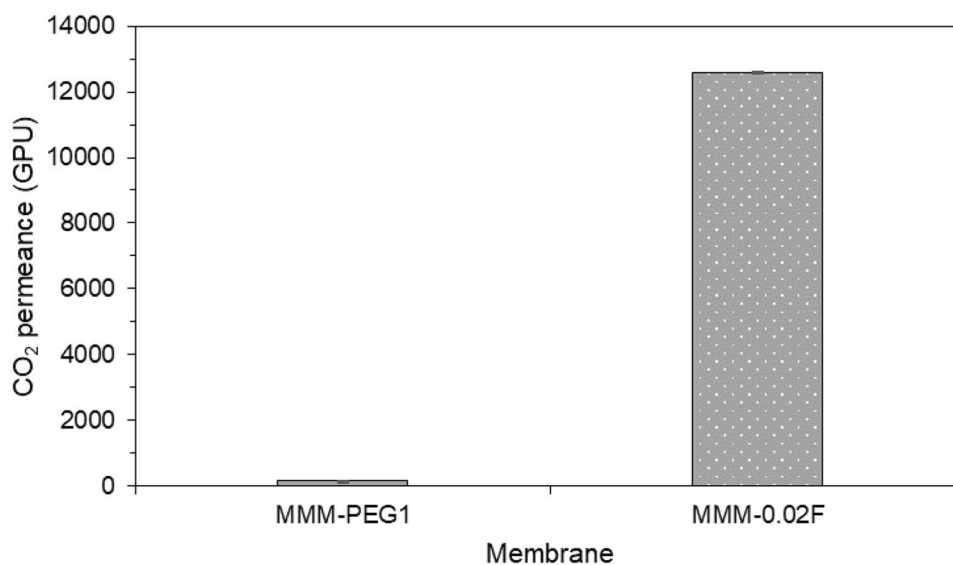
from 20 wt% to 10 wt%, as observed in Fig. 14b and d. Furthermore, the thickness of dense top layer can be seen reduced significantly when PES is decreased to 8 wt%, as seen in Fig. 14f. This is because the dope solution with higher PES content has higher viscosity [34]. Casting solution with higher viscosity reduces the transport rate of nonsolvent, causing a thicker dense top layer to form [35]. Hence, the thickness of dense top layer decreases from MMM-PEG1 to MMM-0.02F and MMM-PEG2.

CO_2 and N_2 separation performance

Based on previous parameter study, MMM incorporated with 0.020 wt% filler loading (MMM-0.02F) has the optimum gas separation performance. Hence, the study on the effect of polymer composition was carried out via single gas permeation test on MMM-PEG1, MMM-0.02F and MMM-PEG2 that has different PEG:PES weight ratio of 20:20, 30:10 and 32:8, respectively with a MWCNTs-F loading of 0.020 wt%. Based on Fig. 15, CO_2 permeance increased dramatically from 166.41 ± 1.16 GPU to $12{,}594.28 \pm 22.77$ GPU when PEG is increased to 30 wt%. The increased PEG content in MMM-0.02F has enhanced permeance because of increased polar ether group that have affinity for CO_2 molecules [5]. With regard to MMM-PEG2, data are not shown as the membrane was not able to build up a minimum pressure of 0.25 bar. This is due to the increased ratio of PEG to PES that weakens the mechanical strength of the membrane [36].

The N_2 permeance for MMM-PEG1 and MMM-0.02F are presented in Fig. 16. According to Fig. 16, the N_2 permeance is 320.39 ± 0.06 and $10{,}197.53 \pm 14.36$ for MMM-PEG1 and MMM-0.02F, respectively. The dramatic increase in permeance attributes to the reduced thickness of dense top layer of MMM-0.02F, as seen in Fig. 14d.

Table 2 Maximum operating pressure of synthesized membrane

Membrane	Maximum operating pressure (bar)
PEG-PES blend	0.25
MMM-0.005F	0.25
MMM-0.01F	0.25
MMM-0.02F	0.25
MMM-0.02P	0.25
MMM-0.03F	0.25
MMM-PEG1	1.20
MMM-PEG2	-

Figure 17 presents the selectivity for MMM-PEG1 and MMM-0.02F. Based on Fig. 17, the CO_2/N_2 selectivity is increased from 0.519 ± 0.007 to 1.235 ± 0.002 when PEG:PES weight ratio is increased from 20:20 (MMM-PEG1) to 30:10 (MMM-0.02F). The increase in CO_2/N_2 is caused by the higher PEG content in MMM-0.02F that has increased sorption sites for CO_2 molecules [5].

Effect of operating pressure

All the synthesized membranes in this research study and their maximum operating pressure are summarized in Table 2. Flue gas generated in the industries are normally at atmospheric pressure (1.01 bar) [1]. Among the membranes summarized in Table 2, MMM-PEG1 are suitable for post-combustion carbon capture in industrial application as it has the mechanical strength to withstand 1.2 bar of pressure, higher than a typical flue gas stream. In contrast, other membranes summarized in Table 2 were not able to withstand a pressure more than 0.25 bar indicating low mechanical strength.

Fig. 15 CO_2 permeance of MMM-PEG1 and MMM-0.02F prepared with different polymer composition at casting thickness of 250 µm at operating pressure of 0.25 bar

Fig. 16 N_2 permeance of MMM-PEG1 and MMM-0.02F prepared at casting thickness of 250 μm at operating pressure of 0.25 bar
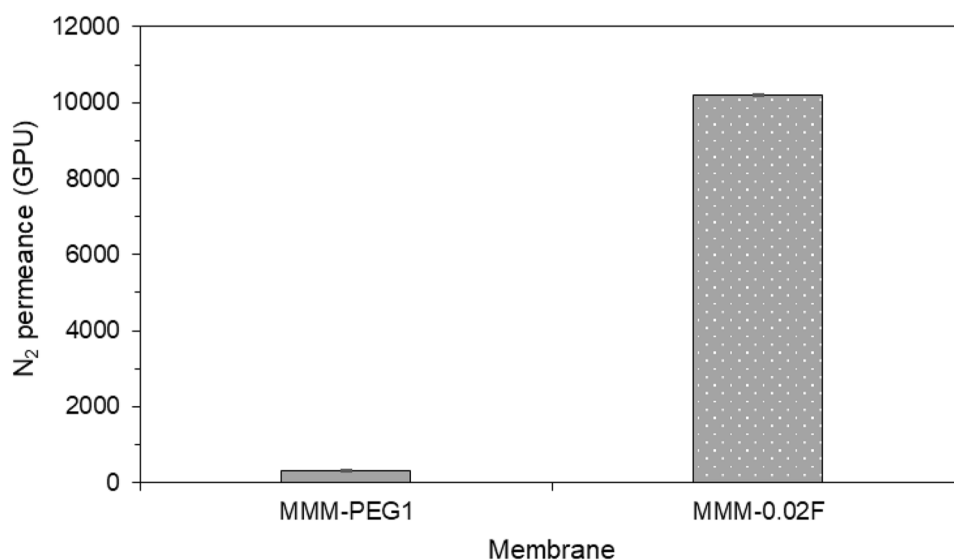
### CO_2 and N_2 separation performance

Single permeation test for CO_2 and N_2 were carried out at different pressure to study the effect of operating pressure on the gas separation properties of MMM-PEG1. Figure 18 presents the CO_2 permeance of MMM-PEG1. Based on Fig. 18, the CO_2 permeance decreased from 166.41 ± 1.16 GPU to 120.17 ± 0.19 GPU when pressure increased from 0.25 bar to 0.50 bar. This is caused by saturation of Langmuir adsorption site [37, 38]. However, when the pressure is increased further to 0.75 bar, 1.00 bar and 1.20 bar, CO_2 permeance increased to 131.19 ± 0.10 GPU, 146.52 ± 0.07 GPU and 185.95 ± 0.55 GPU, respectively. The increase in CO_2 permeance when pressure was further increased may

be due to the increase in CO_2 solubility in rubbery polymer as pressure increases, in this case PEG in MMM-PEG1 [39].

Figure 19 represents the effect of pressure on N_2 permeance of MMM-PEG1. As shown in Fig. 19, the N_2 permeance decreased from 320.39 ± 0.06 GPU (0.25 bar) to 236.09 ± 0.52 GPU, 184.57 ± 0.07 GPU and 169.19 ± 0.70 GPU at 0.50 bar, 0.75 bar and 1.00 bar, respectively. Saturation of Langmuir sorption sites caused the initial decrease of N_2 permeance when pressure was increased [37, 38]. When pressure was further increased to 1.20 bar, the permeance stayed constant at 170.39 ± 0.11 GPU indicating that Henry's law based solution transport becomes dominant in contributing to the gas permeance [38].
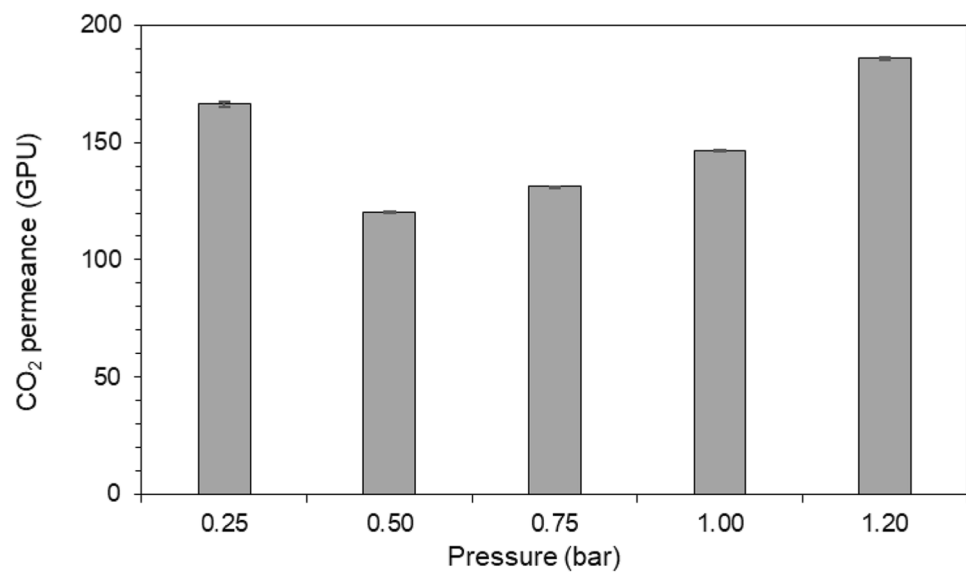
The CO_2/N_2 selectivity for MMM-PEG1 at different operating pressure is presented in Fig. 20. According

Fig. 17 CO_2/N_2 selectivity of MMM-PEG1 and MMM-0.02F prepared at casting thickness of 250 μm at operating pressure of 0.25 bar
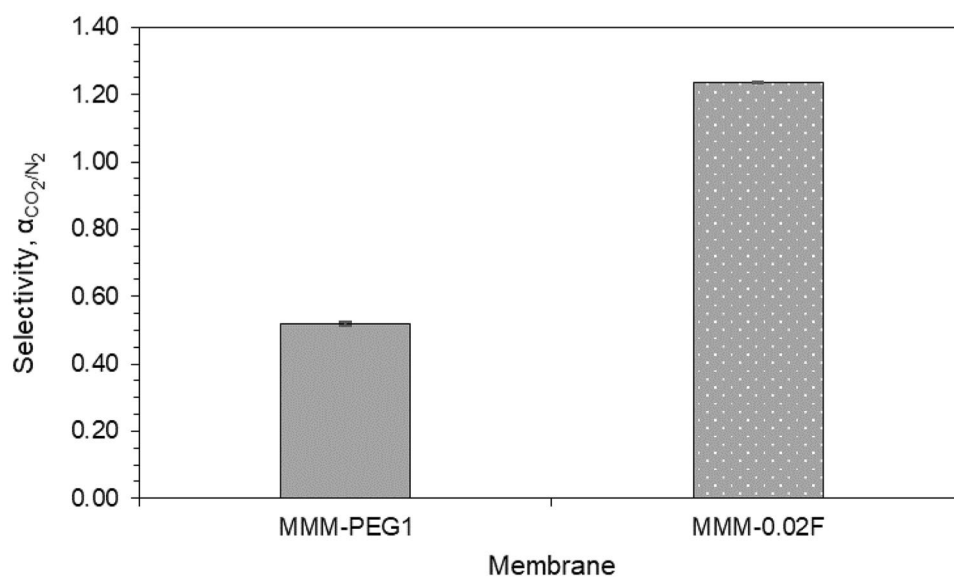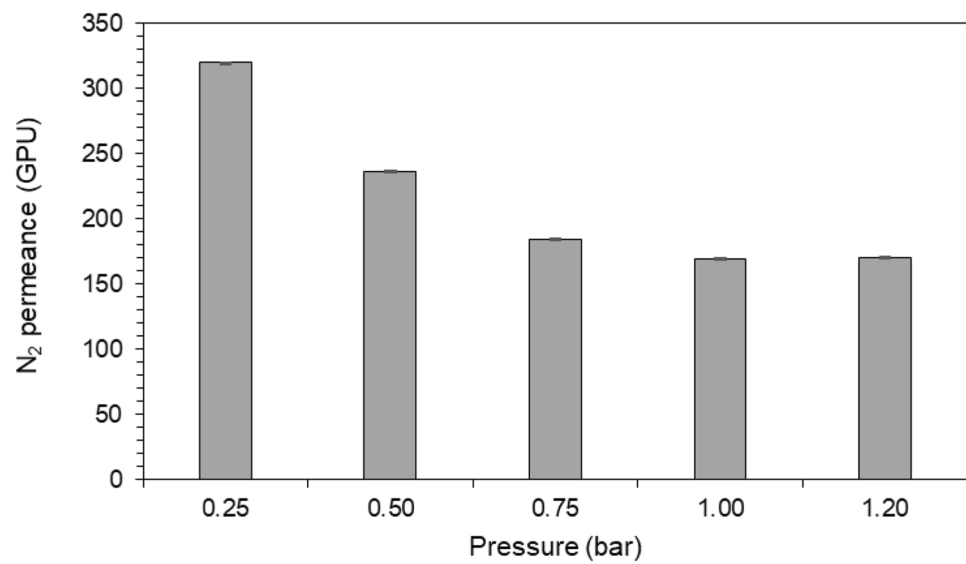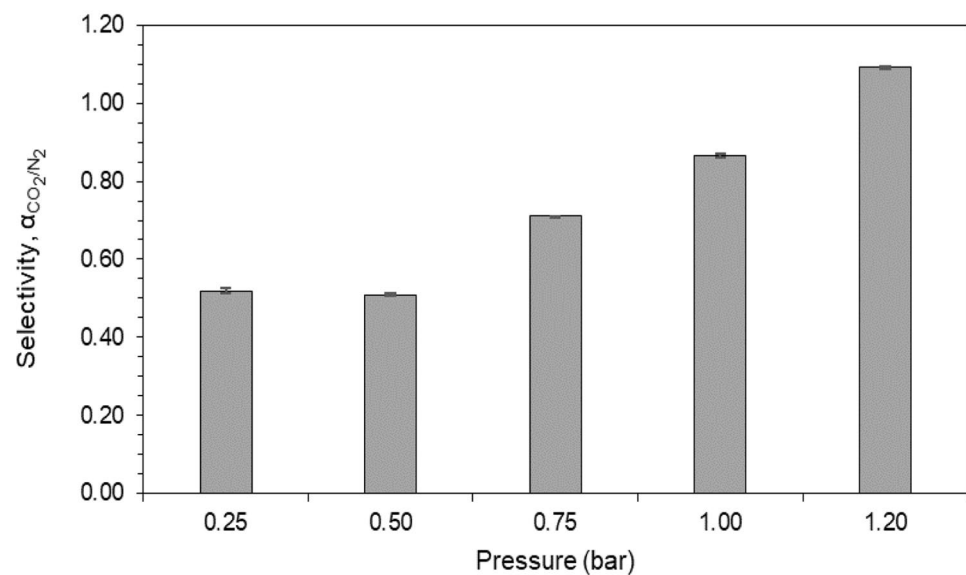
Fig. 18 CO_2 permeance MMM-PEG1 at casting thickness of 250 μm at different operating pressure

Fig. 19 N_2 permeance of MMM-PEG1 at casting thickness of 250 μm at different operating pressure

Fig. 20 CO_2/N_2 selectivity of MMM-PEG1 at casting thickness of 250 μm at different operating pressure

to Fig. 20, MMM-PEG1 has a CO_2/N_2 selectivity of 0.519 ± 0.007, 0.509 ± 0.003, 0.711 ± 0.001, 0.866 ± 0.004 and 1.091 ± 0.03 at an operating pressure of 0.25 bar, 0.50 bar, 0.75 bar, 1.00 bar and 1.20 bar, respectively. The increase in CO_2/N_2 selectivity may be explained by the high affinity of polar ether bond presence in PEG that preferentially adsorb CO_2 molecules compared to N_2 molecules [5].

Conclusion

In conclusions, integration of MWCNTs in PEG-PES blend membrane, MWCNTs content in PEG-PES and polymer concentration are all important factor that plays a role in determining the morphology and gas separation performance of a membrane. Based on experiment, it was found that MWCNTs-F have better gas separation enhancement properties due to its shorter and less agglomerated nature. Furthermore, the optimum MWCNTs-F loading was found to be 0.020 wt% (MMM-0.02F). At 0.020 wt% MWCNTs-F loading, the highest selectivity of 1.235 ± 0.002 was achieved with a CO_2 and N_2 permeance of $12{,}594.28 \pm 22.77$ GPU and $10{,}197.53 \pm 14.36$ GPU, respectively. Furthermore, it was found that at PEG:PES weight ratio of 20:20 (MMM-PEG1), membrane mechanical strength was increased as the membrane can withstand a pressure up to 1.2 bar which is higher than typical flue gas pressure. Thus, it is suitable for post-combustion application in the industry.

References

1. Songolzadeh M, Soleimani M, Takht Ravanchi M, Songolzadeh R et al (2014) Carbon Dioxide Separation from Flue Gases: A Technological Review Emphasizing Reduction in Greenhouse Gas Emissions Sci World J. https://doi.org/10.1155/2014/828131

2. Creamer AE, Gao B (2016) Carbon-based adsorbents for post-combustion CO_2 capture: A critical review. Environ Sci Technol 50(14):7276–7289. https://doi.org/10.1021/acs.est.6b00627

3. He X (2018) A review of material development in the field of carbon capture and the application of membrane-based processes in power plants and energy-intensive industries. Energy Sustain Soc 8(1):1–14. https://doi.org/10.1186/s13705-018-0177-9

4. Hamid MRA, Jeong H-K (2018) Recent advances on mixed-matrix membranes for gas separation: Opportunities and engineering challenges. Korean J Chem Eng 35(8):1577–1600. https://doi.org/10.1007/s11814-018-0081-1

5. Akbarian I, Fakhar A, Ameri E, Sadeghi M et al (2018) Gas-separation behavior of poly(ether sulfone)–poly(ethylene glycol) blend membranes. J Appl Polym Sci 135(44):46845. https://doi.org/10.1002/app.46845

6. Low BT, Zhao L, Merkel TC, Weber M, Stolten D et al (2013) A parametric study of the impact of membrane materials and process operating conditions on carbon capture from humidified flue gas. J Membrane Sci 431:139–155. https://doi.org/10.1016/j.memsci.2012.12.014

7. Liu J, Hou X, Park HB, Lin H et al (2016) High-Performance Polymers for Membrane CO_2/N_2 Separation. Chemistry 22(45):15980–15990. https://doi.org/10.1002/chem.201603002

8. Hadi SHAA, Mannan HA, Mukhtar H, Shaharun MS, Murugesan T et al (2016) Morphological analysis of Polyethersulfone/polyvinyl Acetate blend membrane synthesized at various polymer concentrations. Paper presented at the IOP Conf. Ser. Earth Environ, Sci

9. Naderi A, Yong WF, Xiao Y, Chung T-S, Weber M, Maletzko C et al (2018) Effects of chemical structure on gas transport properties of polyethersulfone polymers. Polymer 135:76–84. https://doi.org/10.1016/j.polymer.2017.12.014

10. Mohamed MG, Kuo SW et al (2019) Functional Silica and Carbon Nanocomposites Based on Polybenzoxazines. Macromol Chem Phys 220 (1):1800306-n/a. https://doi.org/10.1002/macp.201800306

11. Samy MM, Mohamed MG, Kuo S-W et al (2020) Pyrene-functionalized tetraphenylethylene polybenzoxazine for dispersing single-walled carbon nanotubes and energy storage. Compos Sci Technol 199:108360. https://doi.org/10.1016/j.compscitech.2020.108360

12. Ahmad AL, Jawad ZA, Low SC, Zein SHS et al (2014) A cellulose acetate/multi-walled carbon nanotube mixed matrix membrane for CO2/N2 separation. J Membrane Sci 451:55–66. https://doi.org/10.1016/j.memsci.2013.09.043

13. Sun H, Wang T, Xu Y, Gao W, Li P, Niu QJ et al (2017) Fabrication of polyimide and functionalized multi-walled carbon nanotubes mixed matrix membranes by in-situ polymerization for CO2 separation. Sep Purif Technol 177:327–336. https://doi.org/10.1016/j.seppur.2017.01.015

14. Zhao N, Liu T, Liu Z, Su Y, Yu H, Ma J, Yang Y, Jiang Z et al (2017) Synthesis and properties of sulfonated biphenyl poly(ether sulfone) and its mixed-matrix membranes containing carbon nanotubes for gas separation. J Appl Polym Sci 134 (29). https://doi.org/10.1002/app.44995

15. Ismail AF, Rahim NH, Mustafa A, Matsuura T, Ng BC, Abdullah S, Hashemifard SA et al (2011) Gas separation performance of polyethersulfone/multi-walled carbon nanotubes mixed matrix membranes. Sep Purif Technol 80(1):20–31. https://doi.org/10.1016/j.seppur.2011.03.031

16. Chen J, Dyer MJ, Yu MF et al (2001) Cyclodextrin-mediated soft cutting of single-walled carbon nanotubes. J Am Chem Soc 123(25):6201. https://doi.org/10.1021/ja015766t

17. Lee RJ, Jawad ZA, Ahmad AL, Chua HB et al (2018) Incorporation of functionalized multi-walled carbon nanotubes (MWCNTs) into cellulose acetate butyrate (CAB) polymeric matrix to improve the CO2/N2 separation. Process Saf Environ 117:159–167. https://doi.org/10.1016/j.psep.2018.04.021

18. Ahmad AL, Jawad ZA, Low SC, Zein SHS et al (2013) The Functionalization of Beta-Cyclodextrins on Multi Walled Carbon Nanotubes: Effects of the Dispersant and Non Aqueous Media. Curr Nanosci 9(1):93–102. https://doi.org/10.2174/1573413711309010015

19. Aroon MA, Ismail AF, Matsuura T et al (2013) Beta-cyclodextrin functionalized MWCNT: A potential nano-membrane material for mixed matrix gas separation membranes development. Beta-cyclodextrin functionalized MWCNT: A potential nano-membrane material for mixed matrix gas separation membranes development 115:39–50

20. Alenazi AN, Hussein AM, Alamry AK, Asiri MA et al (2018) Nanocomposite-Based Aminated Polyethersulfone and

Carboxylate Activated Carbon for Environmental Application. A Real Sample Analysis. C 4 (2). https://doi.org/10.3390/c4020030

21. Chieng BW, Ibrahim NA, Yunus WMZW, Hussein MZ et al (2014) Poly(lactic acid)/Poly(ethylene glycol) Polymer Nanocomposites: Effects of Graphene Nanoplatelets. Polymers 6(1):93–104. https://doi.org/10.3390/polym6010093

22. He Y, Xu Z, Yang Q, Wu F, Liang L et al (2015) Supramolecular modification of multi-walled carbon nanotubes with β-cyclodextrin for better dispersibility. J Nanopart Res 17(1):1–10. https://doi.org/10.1007/s11051-015-2866-z

23. Del Valle EMM (2004) Cyclodextrins and their uses: a review. Process Biochem 39(9):1033–1046. https://doi.org/10.1016/S0032-9592(03)00258-9

24. Guillen GR, Pan Y, Li M, Hoek EMV et al (2011) Preparation and Characterization of Membranes Formed by Nonsolvent Induced Phase Separation: A Review. Ind Eng Chem Res 50(7):3798–3817. https://doi.org/10.1021/ie101928r

25. Guillen GR, Ramon GZ, Pirouzkavehpour H, Kaner RB, Hoek EMV et al (2013) Direct Microscopic Observation of Membrane Formation by Nonsolvent Induced Phase Separation. J Membrane Sci 431:212–220. https://doi.org/10.1016/j.memsci.2012.12.031

26. Khorsand-Ghayeni M, Barzin J, Zandi M, Kowsari M et al (2017) Fabrication of asymmetric and symmetric membranes based on PES/PEG/DMAc. Polym Bull 74(6):2081–2097. https://doi.org/10.1007/s00289-016-1823-z

27. Khan M, Filiz V, Bengtson G, Shishatskiy S, Rahman M, Abetz V et al (2012) Functionalized carbon nanotubes mixed matrix membranes of polymers of intrinsic microporosity for gas separation. Nanoscale Res Lett 7(1):1–12. https://doi.org/10.1186/1556-276X-7-504

28. Wong KC, Goh PS, Ismail AF et al (2018) Carbon-Based Nanocomposite Membrane for Acidic Gas Separation. In: Ismail AF, Goh PS (eds) Carbon-Based Polymer Nanocomposites for Environmental and Energy Applications. Elsevier, pp 233–260. https://doi.org/10.1016/B978-0-12-813574-7.00010-1

29. Aroon MA, Ismail AF, Montazer-Rahmati MM, Matsuura T et al (2010) Effect of Raw Multi-Wall Carbon Nanotubes on Morphology and Separation Properties of Polyimide Membranes. Sep Sci Technol 45(16):2287–2297. https://doi.org/10.1080/01496395.2010.484007

30. Ge L, Zhu Z, Rudolph V et al (2011) Enhanced gas permeability by fabricating functionalized multi-walled carbon nanotubes and polyethersulfone nanocomposite membrane. Sep Purif Technol 78(1):76–82. https://doi.org/10.1016/j.seppur.2011.01.024

31. Neoh T-L, Yoshii H, Furuta T et al (2006) Encapsulation and Release Characteristics of Carbon Dioxide in α-Cyclodextrin. J Incl Phenom Macrocycl Chem 56(1):125–133. https://doi.org/10.1007/s10847-006-9073-6

32. Narayanan G, Shen J, Boy R, Gupta BS, Tonelli AE et al (2018) Aliphatic Polyester Nanofibers Functionalized with Cyclodextrins and Cyclodextrin-Guest Inclusion Complexes. Polymers 10(4):428. https://doi.org/10.3390/polym10040428

33. Shimekit B, Mohd Shariff A, Mukhtar H, Bustam MA, Elkhalifah AEI, Ullah S, Riaz N et al (2014) Interfacial Defects on Mixed Matrix Membranes and Mitigation Techniques for Gas Separation: A Review. Appl Mech Mater 625(3):653–656. https://doi.org/10.4028/www.scientific.net/AMM.625.653

34. Liu X, Liu H, Li P et al (2017) Effect of Polymer Dope Concentration on the Morphology and Performance of PES/PDMS Hollow Fiber Composite Membrane for Gas Separation. Juniper Online J Mater Sci 1 (5):555573. https://doi.org/10.19080/JOJMS.2017.01.555573

35. Ding C, Yin J, Deng B et al (2014) Effects of Polysulfone (PSf) Support Layer on the Performance of Thin-Film Composite (TFC) Membranes. J Chem Proc Eng 1:1–8

36. Ma Y, Shi F, Ma J, Wu M, Zhang J, Gao C et al (2011) Effect of PEG additive on the morphology and performance of polysulfone ultrafiltration membranes. Desalination 272(1):51–58. https://doi.org/10.1016/j.desal.2010.12.054

37. Moli Z, Liming D, Dongxiao X, Bing C, Seyed Saeid H, Pei L et al (2019) Approaches to Suppress CO2-Induced Plasticization of Polyimide Membranes in Gas Separation Applications. Processes 7(1):51. https://doi.org/10.3390/pr7010051

38. Lasseuguette E, Malpass-Evans R, Carta M, McKeown NB, Ferrari M-C et al (2018) Temperature and Pressure Dependence of Gas Permeation in a Microporous Tröger's Base Polymer. Membranes 8(4):132. https://doi.org/10.3390/membranes8040132

39. Fam W, Mansouri J, Li H, Chen V et al (2017) Improving CO_2 separation performance of thin film composite hollow fiber with Pebax®1657/ionic liquid gel membranes. J Membrane Sci 537:54–68. https://doi.org/10.1016/j.memsci.2017.05.011